Upper tropospheric ozone between latitudes 60S and 60N derived from Nimbus 7 TOMS/THIR Cloud Slicing

J. R. Ziemke, S. Chandra, and P. K. Bhartia

Code 916, NASA Goddard Space Flight Center, Greenbelt, Maryland

Abstract. This study evaluates the spatial distributions and seasonal cycles in upper tropospheric ozone (pressure range 200-500 hPa) from low to high latitudes (60S to 60N) derived from the satellite retrieval method called "Cloud Slicing." Cloud Slicing is a unique technique for determining ozone profile information in the troposphere by combining co-located measurements of cloud-top pressure and above-cloud column ozone. For upper tropospheric ozone, co-located measurements of Nimbus 7 Total Ozone Mapping Spectrometer (TOMS) above-cloud column ozone and Nimbus 7 Temperature Humidity Infrared Radiometer (THIR) cloud-top pressure during 1979-1984 were incorporated. In the tropics, upper tropospheric ozone shows year-round enhancement in the Atlantic region and evidence of a possible semiannual variability. Upper tropospheric ozone outside the tropics shows greatest abundance in winter and spring seasons in both hemispheres with largest seasonal and largest amounts in the NH. These characteristics are similar to lower stratospheric ozone. Comparisons of upper tropospheric column ozone with both stratospheric ozone and a proxy of lower stratospheric air mass (i.,e., tropopause pressure) from National Centers for Environmental Prediction (NCEP) suggest that stratosphere-troposphere exchange (STE) may be a significant source for the seasonal variability of upper tropospheric ozone almost everywhere between 60S and 60N except in low latitudes around 10S to 25N where other sources (e.g., tropospheric transport, biomass burning, aerosol effects, lightning, etc.) may have a greater role.

1. Introduction.

The first assessment of tropospheric column ozone (TCO) derived from satellite measurements was based on the residual method of *Fishman et al.* [1990] which subtracted SAGE stratospheric column ozone (SCO) from TOMS total column ozone to determine TCO. Although it was demonstrated that this method could retrieve information of TCO distributions extending from the tropics to middle latitudes, essentially only a climatology of TCO was obtainable because of the sparse solar occultation measurements of stratospheric ozone profiles available from SAGE (around 1 to 2 local profile measurements per month). In addition it was noted by *Fishman et al.* [1990] that this method had further difficulties caused by subtracting two large column ozone measurements from two independent instruments (i.e., TOMS and SAGE) which were not inter-calibrated.

Subsequently, a number of algorithms based on tropospheric ozone residual methods were developed with significant improvements in characterizing the seasonal, interannual, and spatial variations of TCO in the tropics [e.g., *Jiang and Yung*, 1996; *Kim and Newchurch*, 1996; *Hudson and Thompson*, 1998; *Ziemke et al.*, 1998; *Thompson and*

Hudson, 1999; *Fishman and Balok*, 1999; *Kim et al.*, 2001; *Ziemke et al.*, 2001]. The TCO derived from these techniques have yielded many important scientific results including characterization of ozone enhancement in the Atlantic during southern spring [first identified by *Fishman et al.*, 1987], evidence of an El Nino signal [*Chandra et al.*, 1998, *Thompson et al.*, 2001], solar cycle forcing [*Chandra et al.*, 1999], characterization of seasonal and interannual variabilities [*Ziemke and Chandra*, 1999], identification of lightning-generated TCO distributions [*Martin et al.*, 2001], and a tropical Atlantic Paradox [*Thompson et al.*, 2001]. Additional studies have shown that the September-October Atlantic maximum and/or the El Nino increase of tropospheric ozone over Indonesia in 1997 were well captured in 3D photochemical transport models [e.g., *Moxim and Levy*, 2000; *Sudo et al.*, 2001; *Bey et al.*, 2001; *Martin et al.*, 2002; *Chandra et al.*, 2002a].

While much has been learned about tropical TCO from various satellite retrieval methods, the extension of measurements and the characterization of TCO outside the tropics has had limited success. The residual method of *Fishman et al.* [1990] was more recently applied by replacing SAGE measurements with solar backscatter ultraviolet (SBUV) to determine SCO [*Vukovich et al.*, 1996; *Fishman and Balok*, 1999]. Unlike SAGE the SBUV profiles provide daily measurements of SCO over much of the globe. However SCO derived from SBUV has limited success because of poor vertical resolution of ozone profile information in the vicinity of the tropopause. *Fishman and Balok* [1999] provided an improvement to this TOMS/SBUV residual technique by applying a normalization to the SBUV profile measurements using ozonesonde climatology [*Logan*, 1999].

The Cloud Slicing technique [*Ziemke et al.*, 2001] provides a method for deriving ozone in the upper troposphere over much of the Earth wherever sufficient clouds exist and co-located measurements of above-cloud column ozone and cloud-top pressures are available. The Nimbus 7 TOMS instrument determines total column ozone in the atmosphere from measuring backscattered UV radiances at six wavelengths varying from 313 nm to 380 nm. Optically thick water vapor clouds in the troposphere are opaque at these UV wavelengths, and as a result the column ozone amount actually measured by TOMS in the presence of such clouds is "above-cloud" column ozone. Cloud Slicing takes advantage of the opaque nature of these thick clouds and above-cloud column ozone measurements to estimate ozone abundance in the troposphere. With this method, above-cloud column ozone is plotted versus co-located cloud-top pressure for a chosen geographical region and for a pre-selected pressure band. The mean slope of the distribution directly yields mean ozone volume mixing ratio.

The current study derives upper tropospheric ozone volume mixing ratio in the pressure range 200-500 hPa between latitudes 60S to 60N and characterizes both spatial patterns and seasonal variabilities present in the data. Although not the main objective, we also investigate possible implications for stratosphere-troposphere exchange (STE) by comparing spatial distributions and seasonal cycles in upper tropospheric ozone with lower stratospheric ozone from UARS Halogen Occultation Experiment (HALOE),

TOMS total column ozone measurements, and lower stratospheric air mass derived from NCEP re-analyses. Ozone in the upper troposphere and lower stratosphere exhibits lifetimes of months to years, respectively. In these regions ozone is a chemical tracer of air mass motion and distribution. One may expect that upper tropospheric ozone, lower stratospheric ozone, and lower stratospheric air mass will show similar seasonal cycles with the occurrence of STE.

The following sections begin with a description of the data and an overview of the Cloud Slicing method, followed by ozonesonde validation of measurements, characterization of seasonal cycles and spatial distributions, correlations of seasonal cycles, and finally a Summary.

2. Nimbus 7 Data and Cloud Slicing.

Nimbus 7 Temperature Humidity and Infrared Radiometer (THIR) cloud-top pressure and Nimbus 7 TOMS version 7 column ozone level-2 footprint measurements were combined to determine upper tropospheric ozone from the method of Cloud Slicing [*Ziemke et al.*, 2001]. The THIR instrument provides thermal emission measurements in a 2 μm-wide channel centered about 11.5 μm to determine cloud-top temperature. THIR cloud-top pressure was derived from temperature using National Centers for Environmental Prediction (NCEP) analyses. Monthly ensemble averages from Cloud Slicing were derived from daily values from January 1979 through October 1984 between latitudes 60S and 60N (5 degree by 5 degree resolution). The pressure band for Cloud Slicing was chosen following several trial data runs to be 200-500 hPa to optimize both number of measurements and signal-to-noise. In tropical latitudes the tropopause lies around 100 hPa year-round while in middle and high latitudes the tropopause may lie at 300 hPa or greater pressure. Cloud Slicing measurements represent mean ozone volume mixing ratio in the upper troposphere lying between 500 hPa and highest cloud tops limited to 200 hPa in THIR cloud pressure data. In annual cycles the derived distributions of ozone may to first order be interpreted as estimates of mean ozone volume mixing ratio lying between 500 hPa and the tropopause under the premise that ozone is relatively well mixed (i.e., constant mixing ratio) on long time scales in the upper troposphere up to tropopause level. Further details for the Cloud Slicing algorithm are discussed in Appendix A.

Figure 1 shows scatter plots of TOMS above-cloud column ozone versus co-located THIR cloud-top pressure for a grid point located near Wallops, Virginia (38N, 75W). The top three frames are three days in July 1984 and the bottom three frames are days in August 1984. The numbers shown in each scatter plot are the derived ozone volume mixing ratio and 2-sigma uncertainties (in parentheses) in units ppmv. The scatter in these distributions is caused by errors in TOMS above-cloud column measurements and also errors caused by some amount of stratospheric ozone variability over the selected 5 degree by 5 degree region (see Appendix). Some additional scatter in the plots in Figure 1 is caused by errors in converting THIR cloud-top temperature measurements to pressure using NCEP analyses. Future satellite instruments with greater spectral resolution may enable the determination of cloud-top pressure directly instead of having to convert

measured cloud-top temperature to pressure from meteorological analyses. Methods capable of deriving tropopause directly from backscattered UV and visible wavelength radiances include the molecular oxygen dimer (O2-O2) method [S. ****, personal communication, 2002] and the rotational Raman scattering "Ring Effect" [*Joiner and Bhartia*, 1995].

Figure 2 shows the average number of Cloud Slicing measurements per month in this investigation. Several regions have average monthly sampling rates of 3 to 4 values per month which is small, yet still comparable to most ground-based ozonesonde stations (section 3). There are two regions in Figure 2 where there are no measurements at all from Nimbus 7 Cloud Slicing because of an insufficient number of high clouds or high reflectivity scenes: (1) the south Pacific oceanic region west of South America, and (2) the south Atlantic oceanic region lying between South America and Africa.

3. Validation with Ozonesonde Measurements.

Time series of upper tropospheric ozone were compared with similar time series at several ground-based World Ozone and Ultraviolet Radiation Data Center (WOUDC) stations. Figure 3 shows time series comparisons of upper tropospheric ozone at several ground station locations. It is noted that both data sources were constructed as monthly ensembles which do not represent true monthly means. This is because measurements for both sources are scarce with some monthly ensembles having as little as only one day of measurements. Despite data sampling problems, upper tropospheric ozone time series in Figure 3 indicate general agreement in mean amounts and seasonal variability with greatest abundance around spring months and minimum amounts in Autumn in both hemispheres. Figure 4 shows seasonal cycle comparisons of the data plotted in Figure 3, including comparisons at several additional ground-station locations. The station locations in Figure 4 begin in the upper left-most frame for Goose, Canada (53N, 60W) and progress with decreasing latitude from left-to-right and downward by row. Most all of the stations are in the NH extratropics (i.e., Europe, Japan, U.S.) and show largest seasonal variations and mean column amounts in mid-to-high latitudes. The SH stations (last two frames) show a reversal of the seasonal cycle variability with largest ozone around SH spring months.

4. Characterization of Seasonal Cycles and Spatial Distributions.

The primary purpose of this investigation is to extend Cloud Slicing to middle and high latitudes and characterize observed seasonal cycles and spatial distributions of upper tropospheric ozone. Figure 5 shows spatial distributions of 6-year averaged 3-month seasonal means (indicated) of upper tropospheric ozone volume mixing ratio. Largest ozone occurs in winter and spring months in both hemispheres with greater abundance in the NH. The most significant amounts occur in mid-to-high latitudes. In the NH midlatitudes in winter and spring months there is evidence of partial poleward entrapment of upper tropospheric ozone caused by the upper tropospheric wind jets which can act as a partial barrier for meridional transport of air mass in the upper troposphere. In the NH

in winter and spring there are large meridional gradients and enhancements in ozone along wind-driven storm track regions such as the eastern U.S. and the Asian continent extending into the eastern Pacific. In the SH in winter and spring seasons the horizontal gradients and mean amounts in ozone are weaker than winter and spring seasons in the NH. There is also a persistent feature present in each season in the SH subtropics which indicates an enhancement of ozone near South America, Africa, and Australia. In the tropics, enhancement of upper tropospheric ozone is present each season in the Atlantic region from South America to Africa compared to the eastern and western Pacific regions.

The seasonal and spatial characteristics of upper tropospheric ozone in Figure 5 resemble that of total column ozone (Figure 6). We note that the near-global similarity of upper tropospheric ozone and total ozone is not an artifact of the Cloud Slicing algorithm which assumes that stratospheric column ozone is spatially invariant over selected 5 degree by 5 degree regions (i.e., all above-cloud column ozone variability over the region is tropospheric in origin). Contamination from stratospheric ozone variability within the algorithm is limited to intense dynamical regions, particularly the tropospheric wind jet regions which are limited to narrow meandering bands in the subtropics and middle latitudes. The Cloud Slicing algorithm removes outlier data associated with the wind jet regions by applying statistical and column ozone filtering (see Appendix A).

The most coherent similarities between upper tropospheric ozone in Figure 5 and total ozone in Figure 6 occur in the NH in winter and spring months. Most contribution to total column ozone lies in the mid-to-lower stratosphere. Because ozone is generally a long-lived tracer of air mass in both the upper troposphere and lower stratosphere (lifetimes of months to years, respectively), the patterns in Figures 5 and 6 suggest a possible influence from STE (discussed in section 5). Figures 7 and 8 show zonal mean seasonal cycles from the data plotted in Figures 5 and 6. It is noted for the upper tropospheric ozone data in Figure 7 that these are not true zonal means since in several months there are regions without enough suitable clouds for applying the Cloud Slicing method (e.g., see Figure 5 and discussion). Nevertheless, in Figures 7 and 8 both upper tropospheric ozone and total column ozone show similar seasonal variation and latitude dependence. In the tropics seasonal cycles are different in these quantities, and both temporal and meridional variations appear weak. Outside the tropics, mean amounts and meridional gradients are greatest around spring months in both hemispheres.

Figure 9 shows zonal mean upper tropospheric ozone for January 1979-October 1984. As in Figure 7, variabilities in upper tropospheric ozone in Figure 9 show largest latitudinal gradients in the extratropics of both hemispheres with peak amounts around spring months. It is noted that the springtime maximum in upper tropospheric ozone volume mixing ratio in NH middle and high latitudes agrees with the NH ozonesonde assessment of *Logan* [1999] (e.g., her Figure 27 for 300 hPa in mid-to-high latitudes and 200 hPa in the subtropics). Figure 9 indicates a possible semiannual component in the tropics. Peak-to-peak amplitudes of this signal are weak, around 2-4 ppmv. In some years (e.g., 1980-1983) there is evidence of a semiannual oscillation while in other years there is not. A

semiannual component in the tropics may indicate a dynamical and/or photochemical forcing related to the semiannual zenith crossing of the sun in the tropics. Comparisons of the semiannual and annual variations in total column ozone and upper tropospheric ozone are shown in Figure 10. The annual and semiannual amplitudes were derived by applying basic Fourier analysis. Both annual and semiannual components in total ozone and upper tropospheric ozone in Figure 10 compare well in a global sense with annual cycle variations exhibiting larger amplitudes and larger latitudinal gradients.

5. Correlations of Seasonal Cycles.

It has been shown that total ozone and upper tropospheric ozone indicate similar spatial and seasonal cycle variabilities extending from low to high latitudes. A plausible explanation for these coherent temporal and spatial relationships may be STE processes in the atmosphere. It is well known that ozone in the upper troposphere and lower stratosphere is a relatively long-lived chemical tracer (e-folding lifetimes of months to years, respectively) so that even monthly measurements in this study provide valuable insight regarding possible occurrence of STE. Recent studies suggest that tropopause folding and turbulent convection are significant sources for transporting stratospheric air mass into the troposphere [e.g., *Langford et al.*, 1996; *Beekmann et al.*, 1997; *Cho et al.*, 1999; *Eisele et al.*, 1999; *Meloen et al.*, 2001; *Bertin et al.*, 2001; *Fujiwara and Takahashi*, 2001]. The global effects of STE on tropospheric ozone and its seasonal variability may be significant. The 3D model study by *Lelieveld and Dentener* [2000] indicated that upwards of 80% of tropospheric ozone may be ascribed to STE in subtropical-to-high latitudes.

Appenzeller et al. [1996, and references therein] showed that air mass lying in the lowermost stratosphere is fundamental to global STE processes. This study investigates potential STE on observed upper tropospheric ozone seasonal cycles by comparing with both lower stratospheric ozone and lower stratospheric air mass. Air mass abundance in the lowermost stratosphere is parameterized from tropopause pressure (see Appendix B). For lower stratospheric ozone we include measurements from the UARS HALOE instrument. HALOE is a solar occultation instrument which provides profile information of stratospheric ozone from the top of the atmosphere down to the tropopause [*Bruhl et al.*, 1996]. Mean ozone volume mixing ratio from HALOE was calculated for both the 46-100 hPa and 46-215 hPa pressure bands (i.e., together encompassing the lower stratosphere extending from tropics to high latitudes) for the 1993-2000 post-Pinatubo time period. Although for a time period later than 1979-1984 and with sparse temporal and spatial coverage as an occultation instrument, the combined 8 years of HALOE measurements provide retrievals of lower stratospheric column ozone adequate to develop seasonal cycles for this comparison. Figure 11 shows seasonal cycles in HALOE zonal mean ozone volume mixing ratio for the 46-100 hPa pressure band evaluated for 1993-2000. For latitudes less than around 25-30 degrees the 46-100 hPa pressure band represents the lower stratosphere. At higher latitudes the pressure band is more representative of the mid-to-lower stratosphere. Seasonal variabilities of HALOE ozone in Figure 11 are comparable to seasonal variabilities in upper tropospheric ozone in mid-

to-high latitudes (compare Figure 11 with Figure 7).

Figure 12 shows temporal correlations as a function of latitude between upper tropospheric ozone and HALOE (stars, long-dashed curves), TOMS total column ozone (bold), and NCEP tropopause pressure (dotted). Correlation calculations with 46-215 hPa HALOE measurements were not plotted in Figure 12 equatorward of 35 degrees latitude because 215 hPa exceeds tropopause pressure in these lower latitudes in winter and spring months. The correlations in Figure 12 are based on 12 months of zonal mean data at each latitude and therefore prescribe only basic agreement or disagreement between seasonal cycles. Correlation amplitudes exceeding 0.58 pass 95% confidence level (i.e., 5% significance level). Seasonal cycles for upper tropospheric ozone, total ozone, and NCEP tropopause pressure were determined from 1979-1984 data. Seasonal cycles for HALOE lower stratospheric column ozone were evaluated for the 1993-2000 (i.e., post-Pinatubo) time period.

If STE is the dominant source of ozone seasonal variability in the upper troposphere, then all four curves in Figure 12 would conceivably have correlations near +1 at latitudes where this persists. In subtropical-to-high latitudes, NCEP tropopause pressure and both HALOE lower stratospheric ozone and TOMS total ozone measurements all indeed show correlations near +1. However this is not the case in the low latitudes in Figure 12 extending from around 10S to 25N. In these lower latitudes the correlations with NCEP tropopause pressure become negative in the NH tropics and correlations with HALOE and TOMS are greatly reduced to low-to-negative values. The poorest correlations occur in the NH tropics and are caused by a seasonal maximum in upper tropospheric ozone during NH spring season compared to seasonal maxima around NH Autumn months in NCEP tropopause pressure, TOMS total ozone, and HALOE lower stratospheric ozone (note seasonal cycle differences for mean ozone volume mixing ratio in Figures 7 and 11 in the NH tropics). Several potential sources of upper tropospheric ozone could explain the seasonal cycles for latitudes 10S to 25N including biomass burning, biogenic emissions, aerosol influenced photochemistry, tropospheric transport, and cloud lightning [e.g., *Moxim and Levy*, 2000; *Lelieveld and Dentener*, 2000; *Bey et al.*, 2001; *Thompson et al.*, 2001; *Martin et al.*, 2001, 2002].

6. Summary.

This investigation has examined spatial distributions and seasonal cycles in upper tropospheric ozone (pressure range 200-500 hPa) extending from low to high latitudes (60S to 60N) by applying the satellite retrieval method known as "Cloud Slicing". This is a new technique for determining ozone profile information in the troposphere by combining co-located measurements of cloud-top pressure and above-cloud column ozone. Previous investigations have had limited ability in measuring tropospheric ozone beyond tropical latitudes from satellite data. Comparisons between upper tropospheric ozone volume mixing ratio derived from Cloud Slicing and ground-based ozonesondes for 60S to 60N compare well in monthly ensemble time series and seasonal cycles despite sparse measurements available from either data source. These comparisons indicate the

efficacy of this method even as applied to the relatively coarse field-of-view scanning measurements from Nimbus 7 TOMS (50 km by 50 km at Nadir, 100 km by 100 km on average). Future satellite instruments with smaller footprint size and greater spectral resolution than TOMS may provide significant improvements to the Cloud Slicing technique, with larger number of measurements and application to constituents other than ozone.

Upper tropospheric ozone indicates a possible semiannual component variability in the tropics. A semiannual oscillation appears in some years but not in other years which may be a result of poor signal-to-noise with the Nimbus 7 measurements. The existence of a semiannual component in the tropics may indicate a dynamical and/or photochemical forcing related to the twice-per-year zenith crossing of the sun in tropical latitudes.

Spatial patterns in upper tropospheric ozone are similar to total column ozone, particularly in the NH during winter-spring. Given long lifetimes (months to years, respectively) for ozone in the upper troposphere and lower stratosphere, ozone in these regions of the atmosphere is a tracer of air mass movement and distribution. The spatial patterns and seasonal cycles in mid-to-high latitudes in both hemispheres are similar for TOMS total ozone, lower stratospheric ozone from UARS HALOE, NCEP lower stratospheric air mass, and upper tropospheric ozone from TOMS Cloud Slicing. The mean amounts and seasonal variabilities in upper tropospheric ozone in the extratropics are both larger in the NH compared to the SH. These observations along with previous 2D and 3D model results indicate a presence of STE in the extratropics. Our analyses suggest support for the concept of a coupling of the effects of air mass in the lowermost stratosphere (i.e., "middle world") and the meridional circulation which in model results produces largest STE in the extratropics of both hemispheres around spring, minimum STE in autumn, and with greater occurrence in the NH.

Comparisons between lower stratospheric air mass, stratospheric ozone, and upper tropospheric ozone imply that STE does not appear to be a major source for the seasonal variability of ozone in the upper troposphere in low tropical latitudes extending over a broad region from around 10S to 25N. In these latitudes there is poor temporal correlations in seasonal cycles between troposphere and stratosphere, especially in NH tropical latitudes were largest amounts of upper tropospheric ozone from Cloud Slicing occur in spring months. There are several sources for upper tropospheric ozone that could explain the seasonal cycles in low latitudes. These sources include biomass burning, biogenic emissions, aerosol influenced photochemistry, tropospheric transport, cloud lightning, etc. (beyond the extent of this study).

Appendix A: Cloud Slicing Algorithm.

Cloud Slicing was applied to daily ensemble measurements over 5 degree × 5 degree binned regions, and then averaged within each month for the January 1979-October 1984 time period. The chosen latitude coverage of co-located TOMS and THIR footprint measurements extends from 60S to 60N. This reduces difficulties of persistent snow and

ice in the polar regions and also eliminates problems with polar night conditions where there are no TOMS backscattered UV ozone measurements. For the Cloud Slicing technique, footprint measurements (50 km × 50 km at Nadir, around 100 km by 100 km on average) of above-cloud column ozone from Nimbus 7 TOMS are plotted versus co-located measurements of Nimbus 7 THIR cloud-top pressure over a pre-selected pressure band (200-500 hPa in this study). The mean slope of the distribution then directly yields mean volume mixing ratio for ozone within that pressure band. Specifically, mean volume mixing ratio (X, in ppmv) is determined from

$$X = 1.27\ \Delta\Omega/\Delta P, \qquad \text{(A1)}$$

where Ω is above-cloud column ozone (in DU), and P is cloud-top pressure (in hPa). *Eck et al.* [1987] showed for Nimbus 7 TOMS that footprint scenes with reflectivity greater than 0.4 are almost always 100% cloud-filled (i.e., 100% cloud fraction scenes). Only scenes with reflectivity greater than 0.44 were selected in this study to eliminate most partially cloudy footprint scenes. This reflectivity filtering is a relaxation from the more stringent 0.6 value of reflectivity used by *Ziemke et al.* [2001] and provides a greater proportion of scenes for applying Cloud Slicing. Another important parameter is the minimum number of daily co-located measurements of ozone and cloud pressure within each 5 degree × 5 degree region. This number was selected (for adequate statistics) in the present study to be at least 20, and as in *Ziemke et al.* [2001], only computed mixing ratio values greater than the statistical 2-sigma value were retained.

A fundamental assumption with Cloud Slicing is that stratospheric column ozone is invariant over the selected region (i.e., all above-cloud column ozone changes over the region are tropospheric in origin). This condition breaks down in and near strong dynamical regions, particularly the tropospheric wind jet regions where stratospheric column ozone may exhibit large zonal and meridional variability. An additional filter is applied to identify these regions: Following analysis for each daily 5 degree × 5 degree gridded region, only horizontal gradients in above-cloud column ozone ($|\Delta\Omega|$) less than 50 DU were retained in the data base. This number was chosen subjectively following several trial runs with Nimbus 7 Cloud Slicing. It is likely that there is some stratospheric contamination in the retrievals, but these effects are expected to be limited mostly to narrow regions associated with the tropospheric wind jets. The consistency with ozonesonde measurements (section 3) and lack of obvious outliers in these regions suggest that the algorithm does not produce a significant amount of stratospheric ozone gradient contamination in the retrievals. It is noted that it is also possible to identify the wind jet regions using global meteorological analyses such as from NCEP, but there are two reservations for doing this given the type of measurements associated with Cloud Slicing: (1) The analyses have a coarse resolution compared to the size of TOMS footprint measurements, and (2) the analyses must be accurate to within about 100 km to 200 km in identifying the location of the wind jets, otherwise a significant portion of bad data may be retained and good data dispensed with Cloud Slicing.

Appendix B: Column Abundance and Air Mass in the Atmosphere.

One can relate ozone and air mass in the atmosphere in a self-consistent way using the concept of column abundance and the Dobson Unit. The fundamental Dobson Unit definition applies to all constituents in the atmosphere, including the total atmosphere itself where both volume and mass mixing ratio are unitary (100 percent content). One Dobson Unit (DU) is equivalent to 10^{-5} m vertical thickness of constituent under conditions of
standard pressure (1013.25 hPa) and standard temperature (273.16K) [e.g., *Andrews et al.*, 1987, and references therein]. Under this definition, column amount (Ω, in DU) between two pressure surfaces P_1 and P_2 may be determined by integrating volume mixing ratio (X, in units ppmv) over pressure P (in units hPa) from

$$\Omega = 0.79 \int_{P_1}^{P_2} X dP \qquad \text{(B1)}$$

The constant 0.79 in (B1) was derived for upper tropospheric levels [*Ziemke et al.*, 2001], but can be applied to any constituent in the troposphere or stratosphere with at most around 1% relative error. For the total atmosphere, X is a constant (10^6 ppmv) in (B1) which yields a simple relationship for computing the total air column lying between two arbitrary pressure levels P_1 and P_2: $\Omega = 7.9\times10^5(P_2-P_1)$. For the global mean surface terrain pressure (about 990 hPa from NCEP re-analyses) this yields a global mean column amount Ω of 7.8×10^8 DU for the total atmosphere.

Mass associated with column amount Ω is determined by integrating local measurements of Ω over surface area element dS (units m^2):

$$M = \sigma \int_S \Omega dS \qquad \text{(B2)}$$

It is well known that one Dobson Unit is equivalent to 2.69×10^{20} molecules m^{-2} [e.g., *Ziemke et al.*, 2001, and references therein]. This number applies to any individual constituent in the atmosphere including the total atmosphere itself. In (B2), it follows that σ is the surface mass column density (units kg m^{-2} DU^{-1}) and is equivalent to $2.69\times10^{20}\mu/N_A$, where μ is mean molecular weight (48 for ozone, around 29 for the total atmosphere) and N_A is Avogadro's constant (6.022×10^{26} particles $kmol^{-1}$). For the total atmosphere of the Earth, the column amount 7.8×10^8 DU from (B1) applied to (B2) yields a total mass of around 5.2×10^{18} kg. In comparison, for ozone in the atmosphere the average total column is about 300 DU and the total mass of ozone is around 3.3×10^{12} kg.

From (B2), a surface mass density associated with local measurements of Ω is given by $\sigma\Omega$. For NCEP atmospheric air mass this parameter becomes $7.9\times10^5\sigma(P_2-P_1)$. It follows that a proxy for lower stratospheric air mass can be obtained by replacing P_2 with tropopause pressure from NCEP re-analyses and choosing P_1 as an arbitrary constant pressure lying above the tropopause. This investigation uses NCEP tropopause pressure

as a first-order proxy of lower stratospheric air mass for cross-correlations of seasonal cycles with upper tropospheric ozone volume mixing ratio from Cloud Slicing (section 5).
We have incorporated NCEP re-analyses tropopause pressure which invokes the WMO 2K km^{-1} lapse-rate definition [*WMO*, 1957].

References.

Andrews, D. G., J. R. Holton, and C. B. Leovy, *Middle Atmosphere Dynamics*, 489 pp., Academic, San Diego, Calif., 1987.

Appenzeller C., J. R. Holton, and K. H. Rosenlof, Seasonal variation of mass transport across the tropopause, *J. Geophys. Res., 101*, 15,071-15,078, 1996.

Beekmann, M., et al., Stratosphere-troposphere exchange - regional and global tropopause folding occurrence, final report, Task group 3b, EUROTRAC, TOR, 1996.

Beekmann, M., G. Ancellet, S. Blonsky, et al., Regional and global tropopause fold occurrence and related ozone flux across the tropopause, *J. Atmos. Chem., 28*, 29-44, 1997.

Bertin, F., B. Camistron, J. L. Caccia, Mixing processes in a tropopause folding observed by an network of ST radar and lidar, *Ann. Geophys., 19*, 953-963, 2001.

Bey et al., Global modeling of tropospheric chemistry with assimilated meteorology: Model description and evaluation, *J. Geophys. Res., 106,* 23,073-23,095, 2001.

Bruhl, et al., Halogen Occultation Experiment ozone channel validation, *J. Geophys. Res., 101*, 10,217-10,240, 1996.

Chandra, S., J. R. Ziemke, W. Min, and W. G. Read, Effects of 1997-1998 El Nino on tropospheric ozone and water vapor, *Geophys. Res. Lett., 25*, 3867-3870, 1998.

Chandra, S., J. R. Ziemke, and R. W. Stewart, An 11-year solar cycle in tropospheric ozone from TOMS measurements, *Geophys. Res. Lett., 26*, 185-188, 1999.

Chandra S., J. R. Ziemke, P. K. Bhartia, Tropical tropospheric ozone: Implications for dynamics and biomass burning, *J. Geophys. Res.*, in press, 2002a.

Chandra, S., J. R. Ziemke, and R. V. Martin, Tropospheric ozone at tropical and middle latitudes, *J. Geophys. Res.*, submitted, 2002b.

Cho, J. Y. N., R. E. Newell, T. P. Bui, et al., Observations of convective and dynamical instabilities in tropopause folds and their contribution to stratosphere-troposphere exchange, *J. Geophys. Res., 104*, 21,549-21,568, 1999.

Eck, T. F., P. K. Bhartia, P. H. Hwang, and L. L. Stowe, Reflectivity of Earth's surface and clouds in ultraviolet from satellite observations, *J. Geophys. Res., 92*, 4287-4296, 1987.

Eisele, H., H. E. Scheel, R. Sladkovic, and T. Trickl, High-resolution Lidar measurements of stratosphere-troposphere exchange, *J. Atmos. Sci., 56*, 319-330, 1999.

Fishman, J., and J. C. Larsen, Distribution of total ozone and stratospheric ozone in the tropics: Implications for the distribution of tropospheric ozone, *J. Geophys. Res., 92*, 6627-6634, 1987.

Fishman, J., C. E. Watson, J. C. Larsen, and J. A. Logan, Distribution of tropospheric ozone determined from satellite data, *J. Geophys. Res., 95*, 3599-3617, 1990.

Fishman, J., and A. E., Balok, Calculation of daily tropospheric ozone residuals using TOMS and empirically improved SBUV measurements: Application to an ozone pollution episode over the eastern United States, *J. Geophys. Res., 104*, 30,319-30,340, 1999.

Fujiwara, M., and M. Takahashi, Role of the equatorial Kelvin wave in stratosphere-troposphere exchange in a general circulation model, *J. Geophys. Res., 106*, 22,763-22,780, 2001.

Hudson, R. D., and A. M. Thompson, Tropical tropospheric ozone (TTO) from TOMS by a modified-residual method, *J. Geophys. Res., 103*, 22,129-22,145, 1998.

Jiang, Y., and Y. L. Yung, Concentrations of tropospheric ozone from 1979 to 1992 over tropical Pacific South America from TOMS data, *Science, 272*, 714-716, 1996.

Joiner, J., and P. K. Bhartia, The determination of cloud pressures from rotational Raman scattering in satellite backscatter ultraviolet measurements, *J. Geophys. Res., 100*, 23,019-23,026, 1995.

Kim J. H., and M. J. Newchurch, Climatology and trends of tropospheric ozone over the eastern Pacific Ocean: The influences of biomass burning and tropospheric dynamics, *Geophys. Res. Lett., 23*, 3723-3726, 1996.

Kim J. H., M. J. Newchurch, and K. Han, Distribution of tropical tropospheric ozone determined by the scan-angle method applied to TOMS measurements, *J. Atmos. Sci, 58*, 2699-2708, 2001.

Langford, A. O., C. D. Masters, M. H. Proffitt et al., Ozone measurements in a tropopause fold associated with a cut-off low system, *Geophys. Res. Lett., 23*, 2501-2504, 1996.

Lelieveld, J., and F. J. Dentener, What controls tropospheric ozone?, *J. Geophys. Res., 105*, 3531-3551, 2000.

Logan, J. A., An analysis of ozonesonde data for the troposphere: Recommendations for testing 3D models, and development of a gridded climatology for tropospheric ozone, *J. Geophys. Res.*, 1999.

Martin R. V., D. J. Jacob, J. A. Logan, J. R. Ziemke, and R. Washington, Detection of lightning influence on tropical tropospheric ozone, Geophys. Res. Lett., 27, 1639-1642, 2001.

Martin et al., Interpretation of TOMS observations of tropical tropospheric ozone with a global model and in-situ observations, *J. Geophys. Res.*, in press, 2002.

Meloen, J., P. C. Siegmund, and M. Sigmond, A Lagrangian computation of stratosphere-troposphere exchange in a tropopause folding event in the subtropical hemisphere, *Tellus, 53*, 368-379, 2001.

Moxim, W. J., and H. Levy II, A model analysis of tropical South Atlantic Ocean tropospheric ozone maximum: The interaction of transport and chemistry, *J. Geophys. Res., 105*, 17,393,-17,415, 2000.

Sudo, K., and M. Takahashi, Simulation of tropospheric ozone changes during 1997-1998 El Nino: Meteorological impact on tropospheric photochemistry, *Geophys. Res Lett., 28*, 4091-4094, 2001.

Thompson, A. M., and R. D. Hudson, Tropical tropospheric ozone (TTO) maps from Nimbus 7 and Earth Probe TOMS by the modified-residual method: Evaluation with sondes, ENSO signals, and trends from Atlantic regional time series, *J. Geophys. Res., 104*, 26,961-26,975, 1999.

Thompson, A M., B. G. Doddridge, J. C. Witte, R. D. Hudson, W. T. Luke, J. E. Johnston, B. J. Johnston, S. J. Oltmans, and R. Weller, A tropical Atlantic Paradox: Shipboard and satellite views of a tropospheric ozone maximum and wave-one in January-February 1999, *Geophys. Res. Lett., 27*, 3317-3320, 2000.

Vukovich, F. M., V. Brackett, J. Fishman, and J. E. Sickles II, On the feasibility of using the tropospheric ozone residual for nonclimatological studies on a quasi-global scale, *J. Geophys. Res., 101*, 9093-9105, 1996.

Ziemke, J. R., S. Chandra, and P. K. Bhartia, Two new methods for deriving tropospheric column ozone from TOMS measurements: The assimilated UARS MLS/HALOE and convective-cloud differential techniques, *J. Geophys. Res., 103*, 22,115-22,127, 1998.

Ziemke, J. R., and S. Chandra, Seasonal and interannual variabilities in tropical tropospheric ozone J. Geophys. Res., 104, 21,425-21,442, 1999.

Ziemke, J. R., S. Chandra, and P. K. Bhartia, "Cloud Slicing": A new technique to derive upper tropospheric ozone from satellite measurements, *J. Geophys. Res, 106*, 9853-9867, 2001.

Figure Captions.

Figure 1. Scatter plots of TOMS above-cloud column ozone (in Dobson Units) versus co-located THIR cloud-top pressure (in hPa) for a grid point located near Wallops, Virginia (38N, 75W). The top three frames are three days in July 1984 and the bottom three frames are days in August 1984. The numbers shown in each scatter plot are the derived ozone volume mixing ratio and 2-sigma uncertainties (in parentheses) in units ppbv.

Figure 2. Average number of Cloud Slicing measurements per month in this study (see Appendix).

Figure 3. (a) and (b): Monthly ensemble time series for years 1979-1984 at several WOUDC ground station locations (indicated) comparing upper tropospheric ozone from Cloud Slicing with ozonesonde measurements. Units are ppbv.

Figure 4. Seasonal cycles (from years 1979-1984) of monthly ensemble time series of upper tropospheric ozone volume mixing ratio (units ppbv) from several ground station locations (including stations plotted in Figure 3). Cloud Slicing measurements are solid, ozonesonde measurements are designated by circles. Cloud Slicing measurements include $\pm 2\sigma$ statistical uncertainties.

Figure 5. Seasonal averages (DJF, MAM, JJA, SON, indicated in each frame) of TOMS upper tropospheric ozone volume mixing ratio (units ppbv) between 60S and 60N derived from Cloud Slicing. Seasonal averages incorporated 1979-1984 Nimbus 7 TOMS/THIR co-located measurements of above-cloud column ozone and cloud-top pressure.

Figure 6. Same as Figure 5 but for TOMS total column ozone (in Dobson Units).

Figure 7. Latitude versus month zonally averaged seasonal cycles in upper tropospheric ozone volume mixing ratio (units ppbv) from Cloud Slicing. Seasonal cycles were derived from TOMS and THIR co-located measurements for 1979-1984.

Figure 8. Similar to Figure 7, but for TOMS total column ozone in Dobson Units.

Figure 9. Upper tropospheric zonal mean ozone volume mixing ratio for January 1979-December 1984. Units are ppbv.

Figure 10. Comparisons of the annual (left) and semiannual (right) amplitudes in total column ozone (solid) and upper tropospheric ozone (dotted). Annual and semiannual amplitudes were derived by applying basic Fourier analysis to the 1979-1984 monthly ensemble time series data. Units for both annual and semiannual amplitudes are ppbv.

Figure 11. Latitude versus month zonally averaged seasonal cycles in lower stratospheric (46-100 hPa) mean ozone volume mixing ratio (units ppmv) from HALOE measurements.

Figure 12. Latitude-dependent temporal correlations between upper tropospheric ozone and HALOE (dashed, stars), TOMS total column ozone (bold), and NCEP tropopause pressure (dotted). Correlation amplitudes exceeding 0.58 pass 95% confidence level (i.e., 5% significance level). Seasonal cycles for upper tropospheric ozone, total ozone, and NCEP tropopause pressure were determined from 1979-1984 data. Seasonal cycles for HALOE lower stratospheric column ozone were evaluated for the 1993-2000 (i.e., post-Pinatubo) time period.

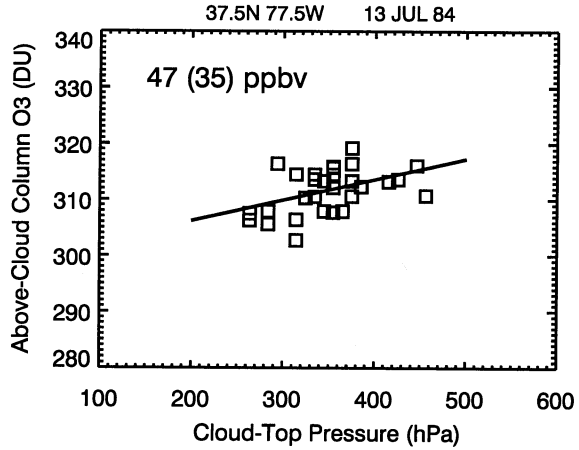
37.5N 77.5W 13 JUL 84
47 (35) ppbv
Above-Cloud Column O3 (DU)
Cloud-Top Pressure (hPa)

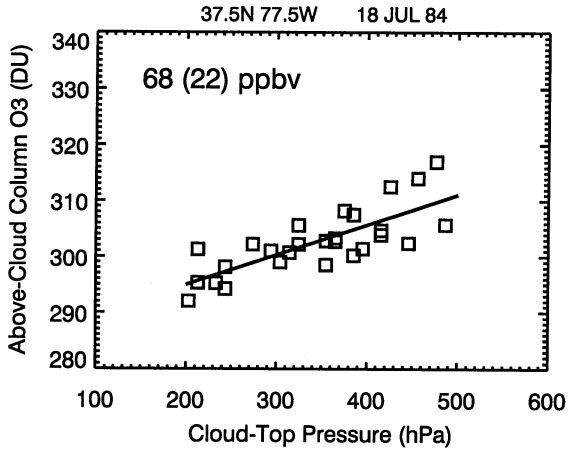
37.5N 77.5W 18 JUL 84
68 (22) ppbv
Above-Cloud Column O3 (DU)
Cloud-Top Pressure (hPa)

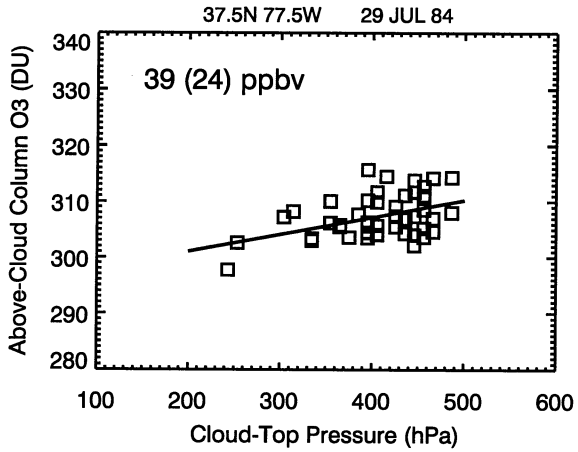
37.5N 77.5W 29 JUL 84
39 (24) ppbv
Above-Cloud Column O3 (DU)
Cloud-Top Pressure (hPa)

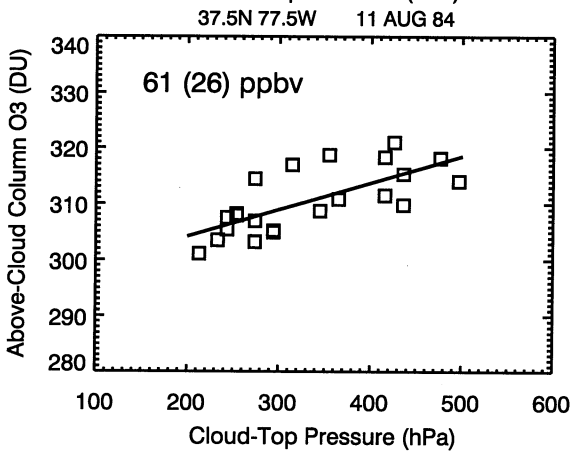
37.5N 77.5W 11 AUG 84
61 (26) ppbv
Above-Cloud Column O3 (DU)
Cloud-Top Pressure (hPa)

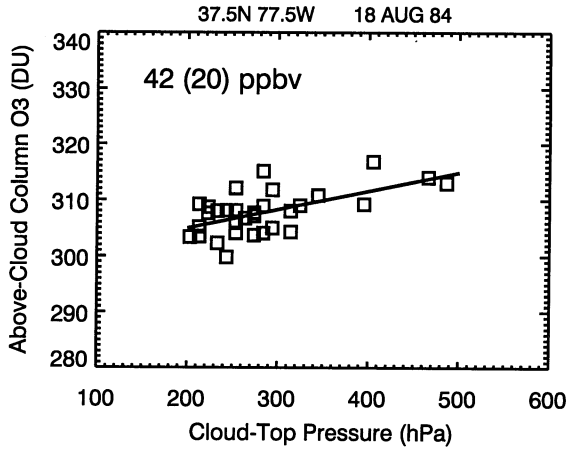
37.5N 77.5W 18 AUG 84
42 (20) ppbv
Above-Cloud Column O3 (DU)
Cloud-Top Pressure (hPa)

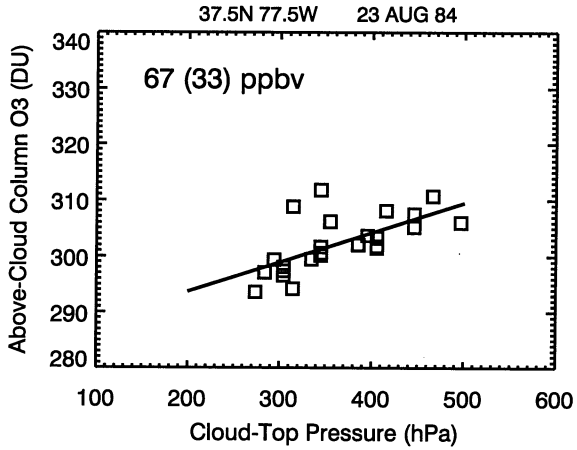
37.5N 77.5W 23 AUG 84
67 (33) ppbv
Above-Cloud Column O3 (DU)
Cloud-Top Pressure (hPa)

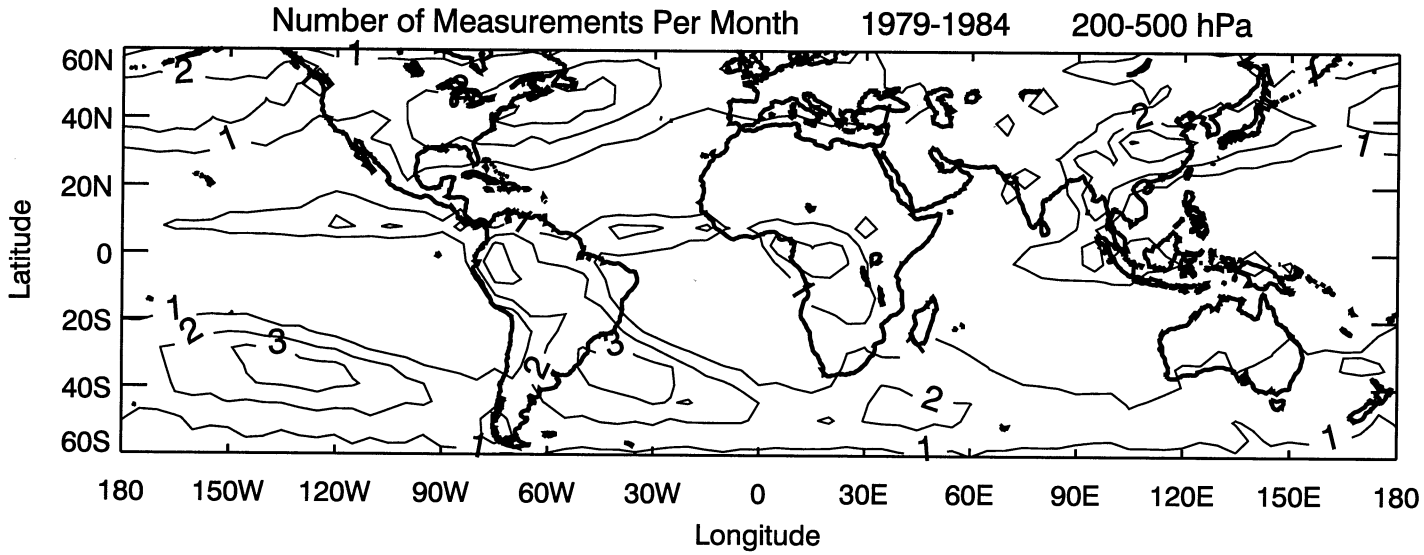
Number of Measurements Per Month 1979-1984 200-500 hPa
60N
40N
20N
0
20S
40S
60S
Latitude
180 150W 120W 90W 60W 30W 0 30E 60E 90E 120E 150E 180
Longitude

F2.

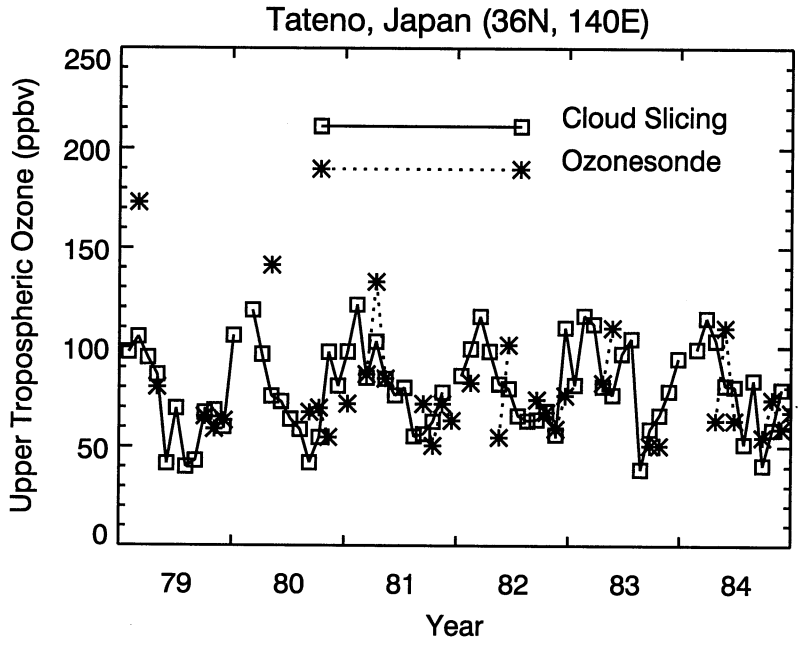
Tateno, Japan (36N, 140E)
Upper Tropospheric Ozone (ppbv)
250
200
150
100
50
0
79
80
81
82
83
84
Year
Cloud Slicing
Ozonesonde

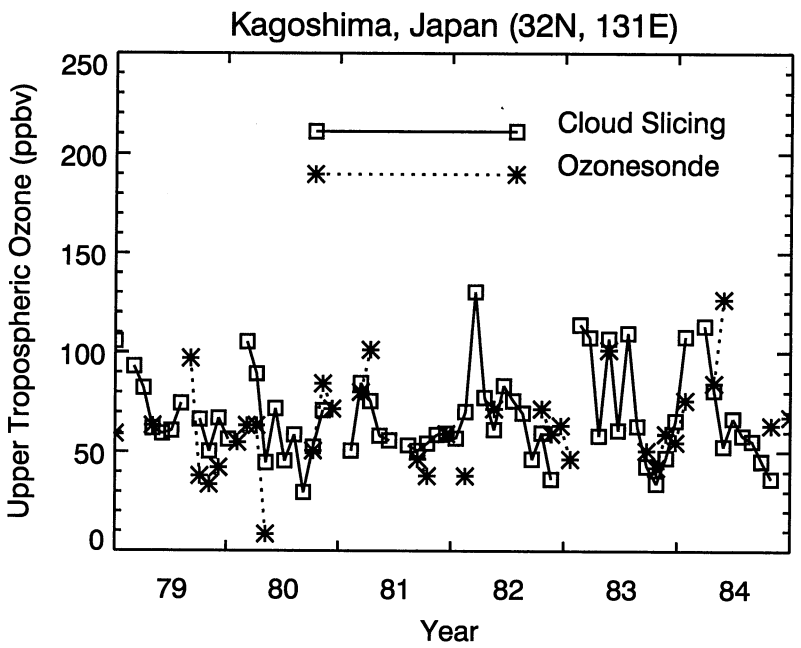
Kagoshima, Japan (32N, 131E)
Upper Tropospheric Ozone (ppbv)
250
200
150
100
50
0
79
80
81
82
83
84
Year
Cloud Slicing
Ozonesonde

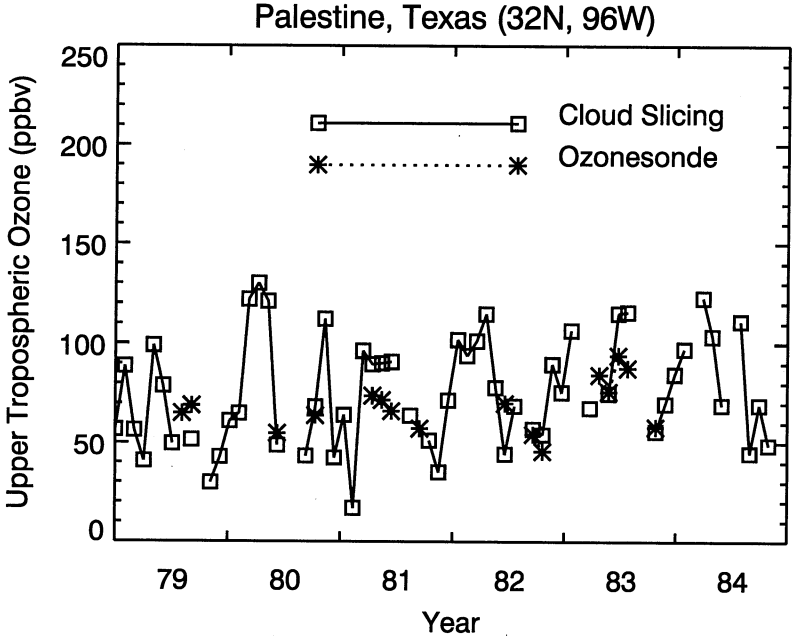
Palestine, Texas (32N, 96W)
Upper Tropospheric Ozone (ppbv)
250
200
150
100
50
0
79
80
81
82
83
84
Year
Cloud Slicing
Ozonesonde

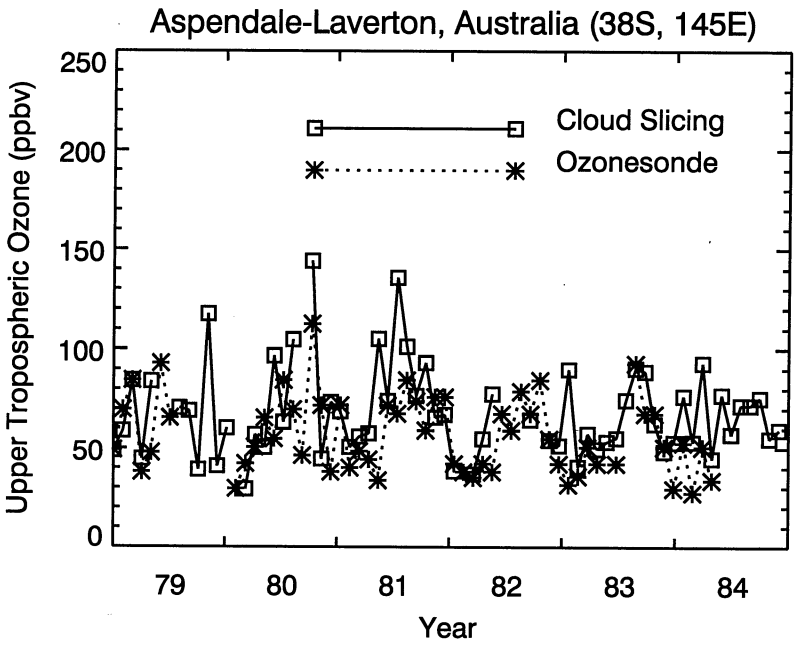
Aspendale-Laverton, Australia (38S, 145E)
Upper Tropospheric Ozone (ppbv)
250
200
150
100
50
0
79
80
81
82
83
84
Year
Cloud Slicing
Ozonesonde

F3a

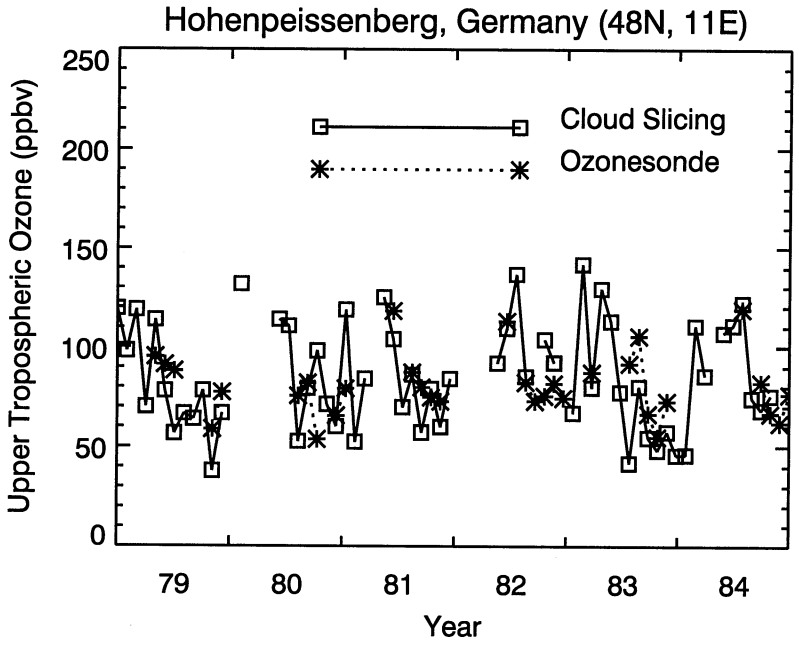
Hohenpeissenberg, Germany (48N, 11E)
Upper Tropospheric Ozone (ppbv)
250
200
150
100
50
0
79
80
81
82
83
84
Year
Cloud Slicing
Ozonesonde

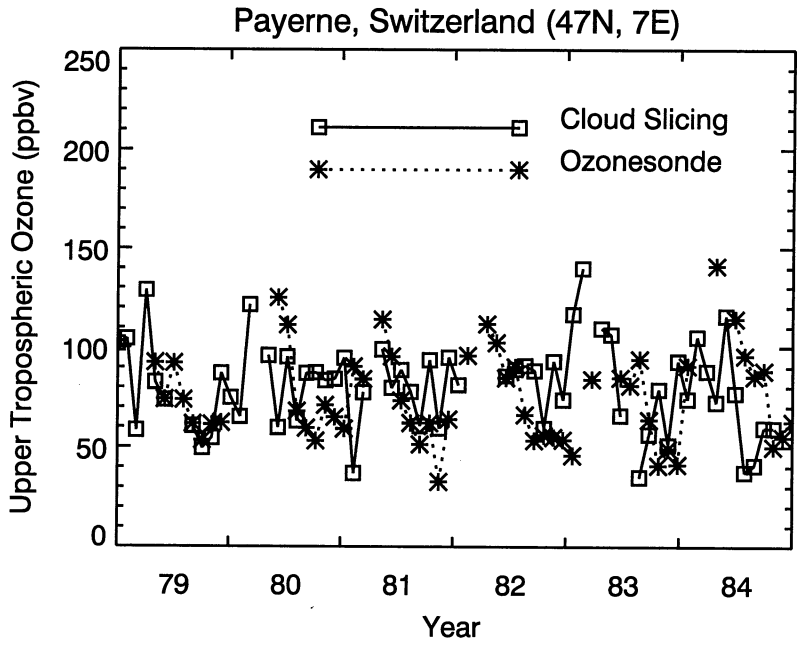
Payerne, Switzerland (47N, 7E)
Upper Tropospheric Ozone (ppbv)
250
200
150
100
50
0
79
80
81
82
83
84
Year
Cloud Slicing
Ozonesonde

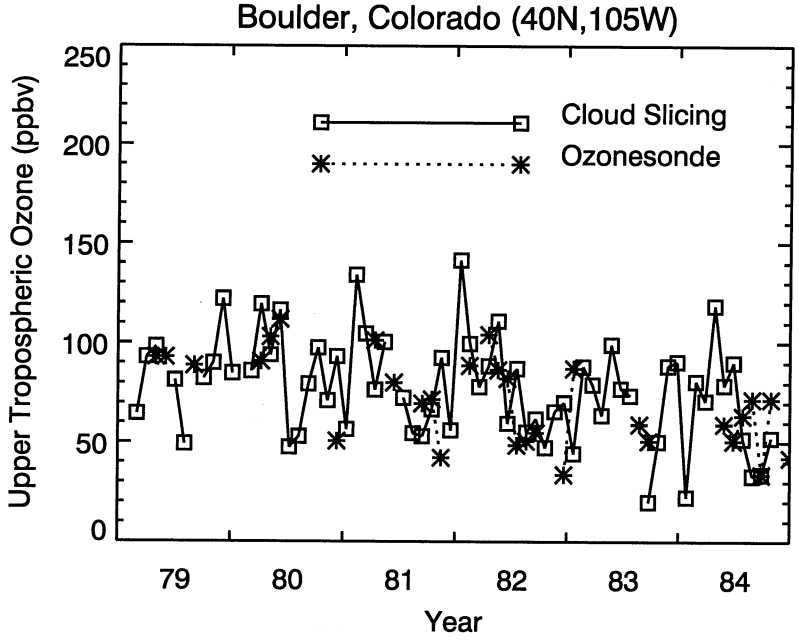
Boulder, Colorado (40N,105W)
Upper Tropospheric Ozone (ppbv)
250
200
150
100
50
0
79
80
81
82
83
84
Year
Cloud Slicing
Ozonesonde

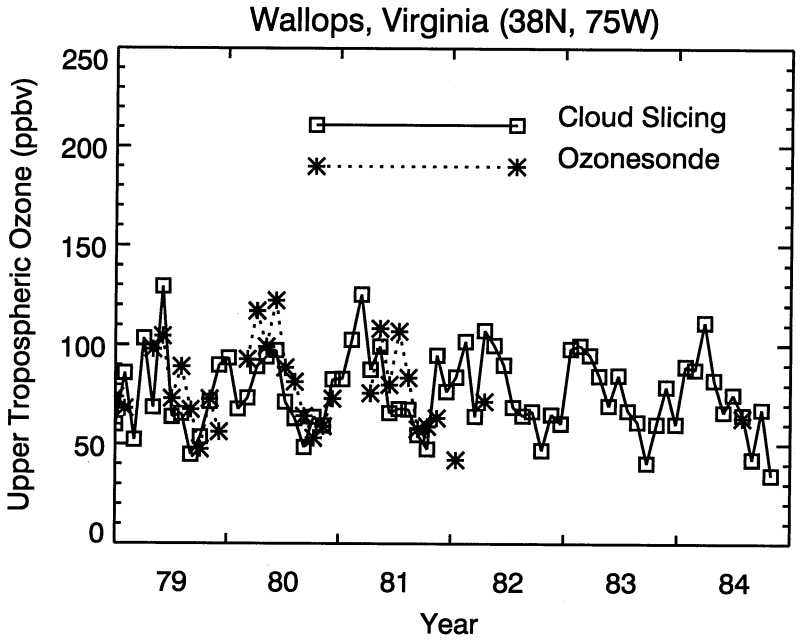
Wallops, Virginia (38N, 75W)
Upper Tropospheric Ozone (ppbv)
250
200
150
100
50
0
79
80
81
82
83
84
Year
Cloud Slicing
Ozonesonde

F31

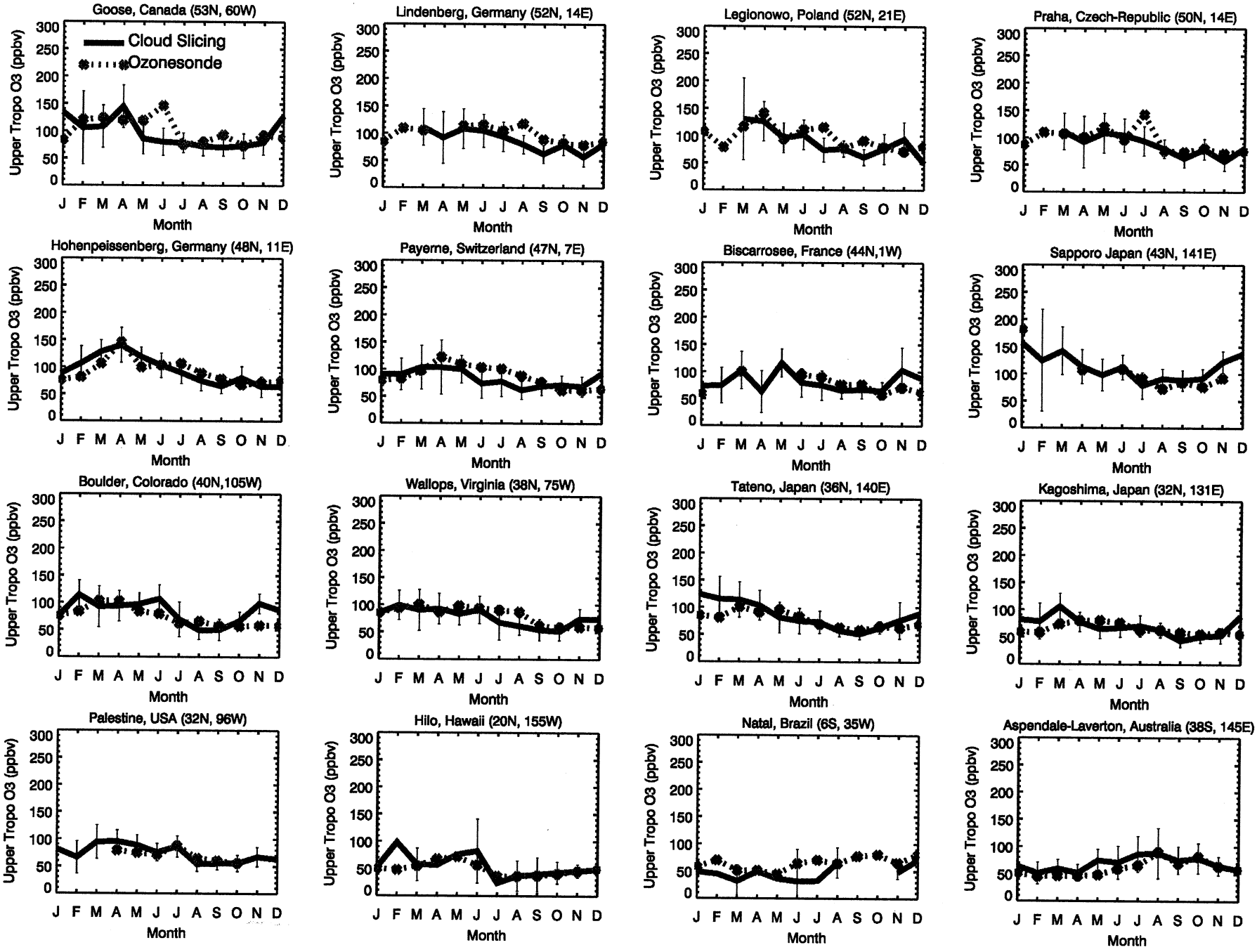
Goose, Canada (53N, 60W)
Cloud Slicing
Ozonesonde
Lindenberg, Germany (52N, 14E)
Legionowo, Poland (52N, 21E)
Praha, Czech-Republic (50N, 14E)
Hohenpeissenberg, Germany (48N, 11E)
Payerne, Switzerland (47N, 7E)
Biscarrosee, France (44N,1W)
Sapporo Japan (43N, 141E)
Boulder, Colorado (40N,105W)
Wallops, Virginia (38N, 75W)
Tateno, Japan (36N, 140E)
Kagoshima, Japan (32N, 131E)
Palestine, USA (32N, 96W)
Hilo, Hawaii (20N, 155W)
Natal, Brazil (6S, 35W)
Aspendale-Laverton, Australia (38S, 145E)
Upper Tropo O3 (ppbv)
0 50 100 150 200 250 300
J F M A M J J A S O N D
Month

UPPER TROPOSPHERIC OZONE (PPBV)

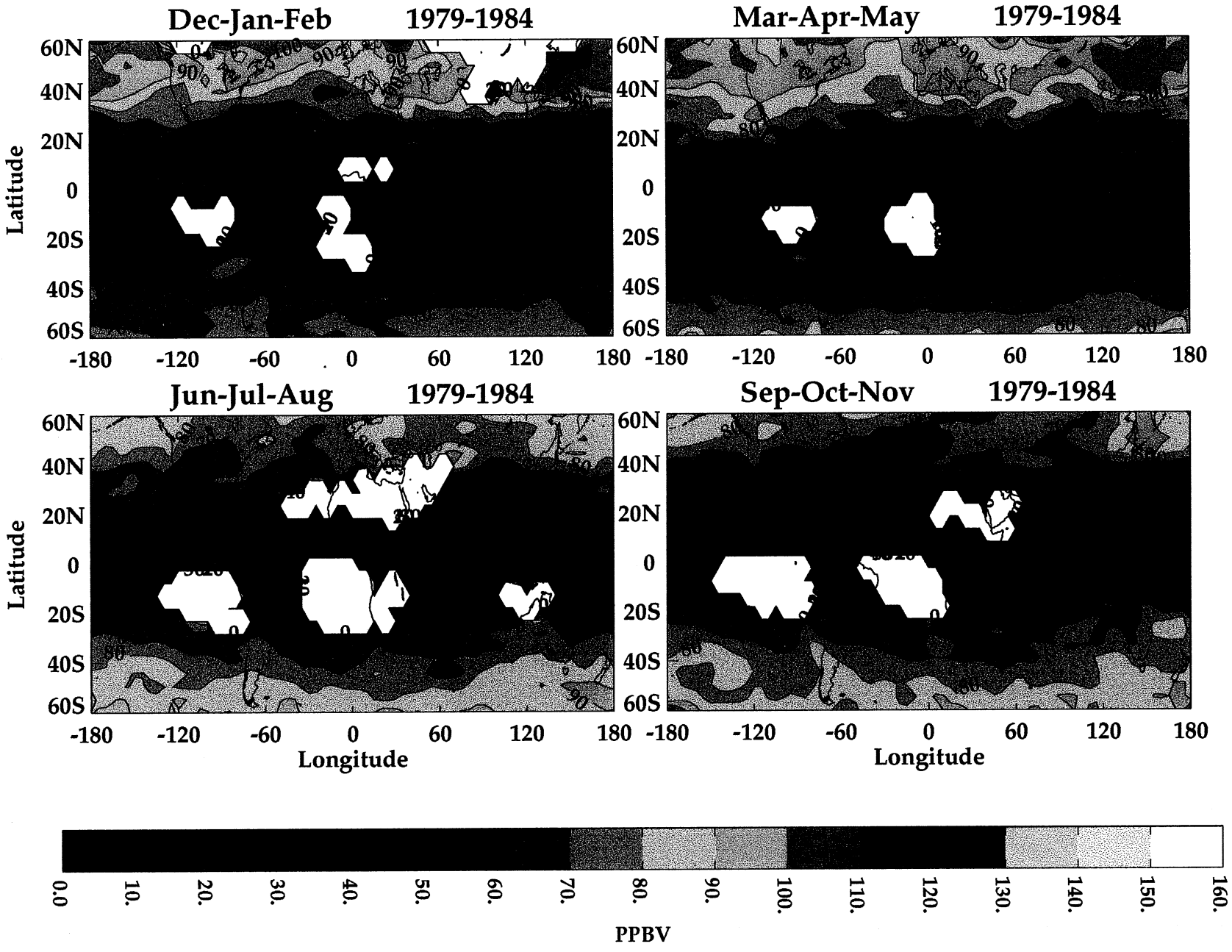

F5

TOTAL COLUMN OZONE (DOBSON UNITS)

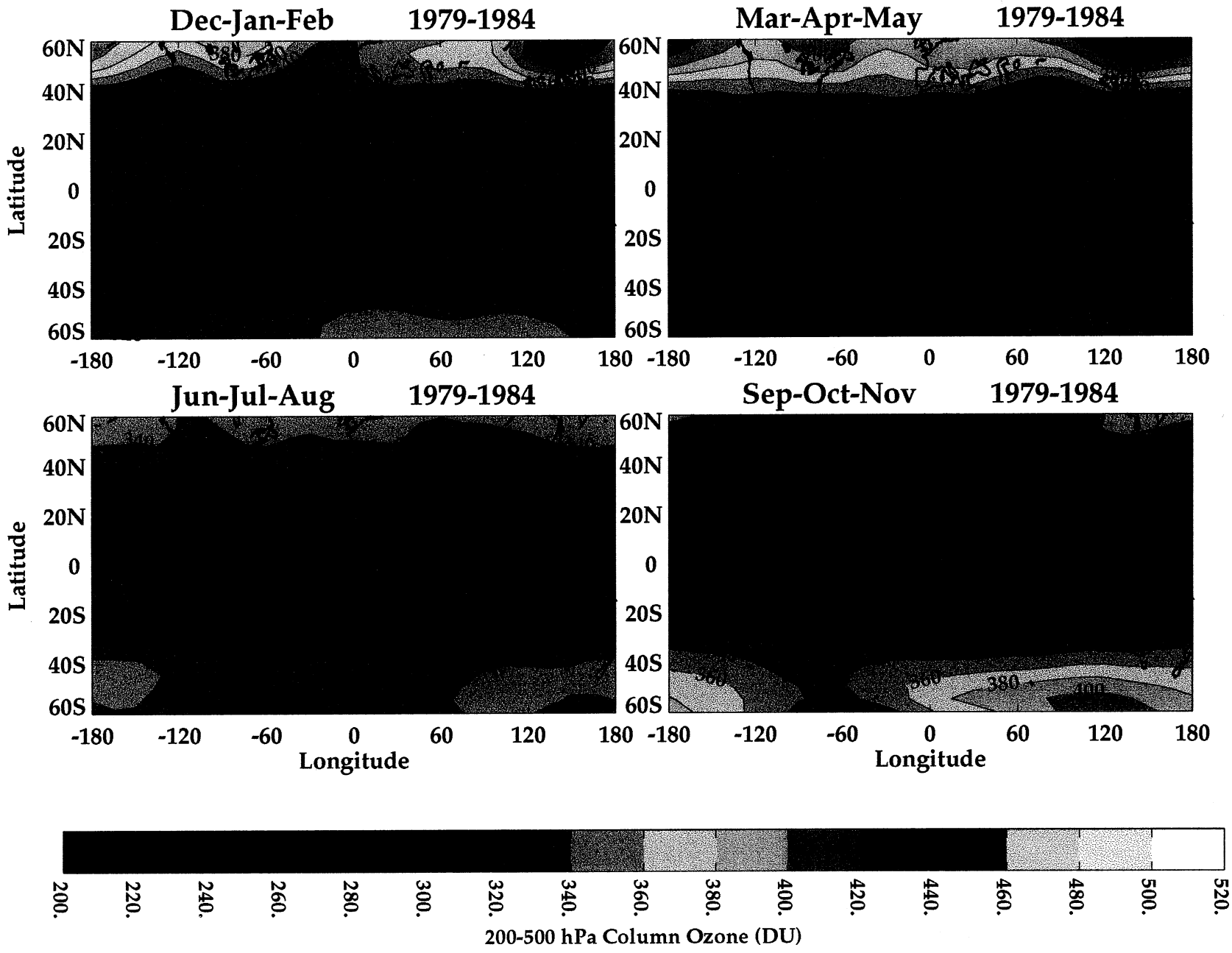

F6

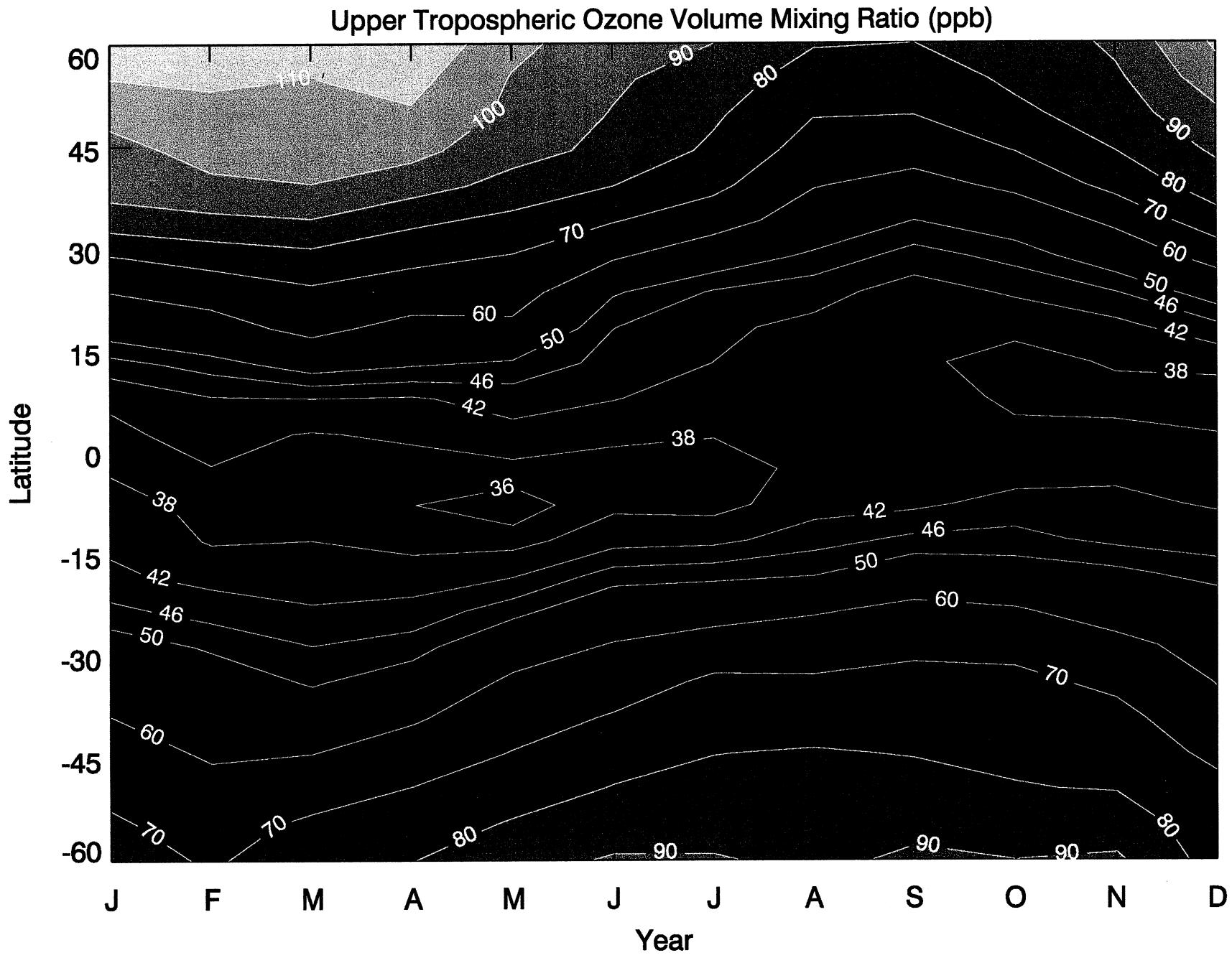
Upper Tropospheric Ozone Volume Mixing Ratio (ppb)
Latitude
60
45
30
15
0
-15
-30
-45
-60
J
F
M
A
M
J
J
A
S
O
N
D
Year
110
100
90
80
70
60
50
46
42
38
36

F7

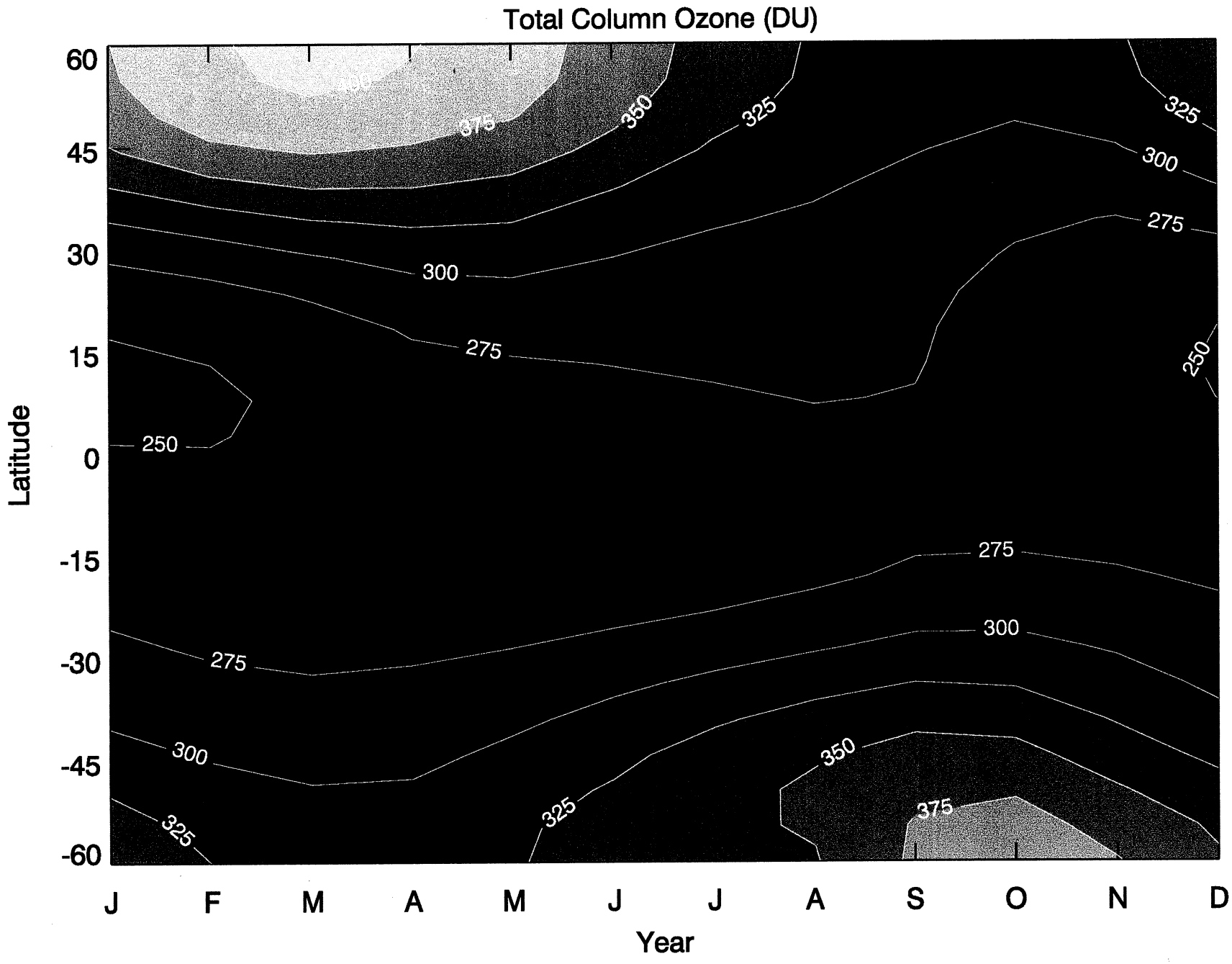
Total Column Ozone (DU)
Latitude
60
45
30
15
0
-15
-30
-45
-60
J
F
M
A
M
J
J
A
S
O
N
D
Year
250
275
300
325
350
375

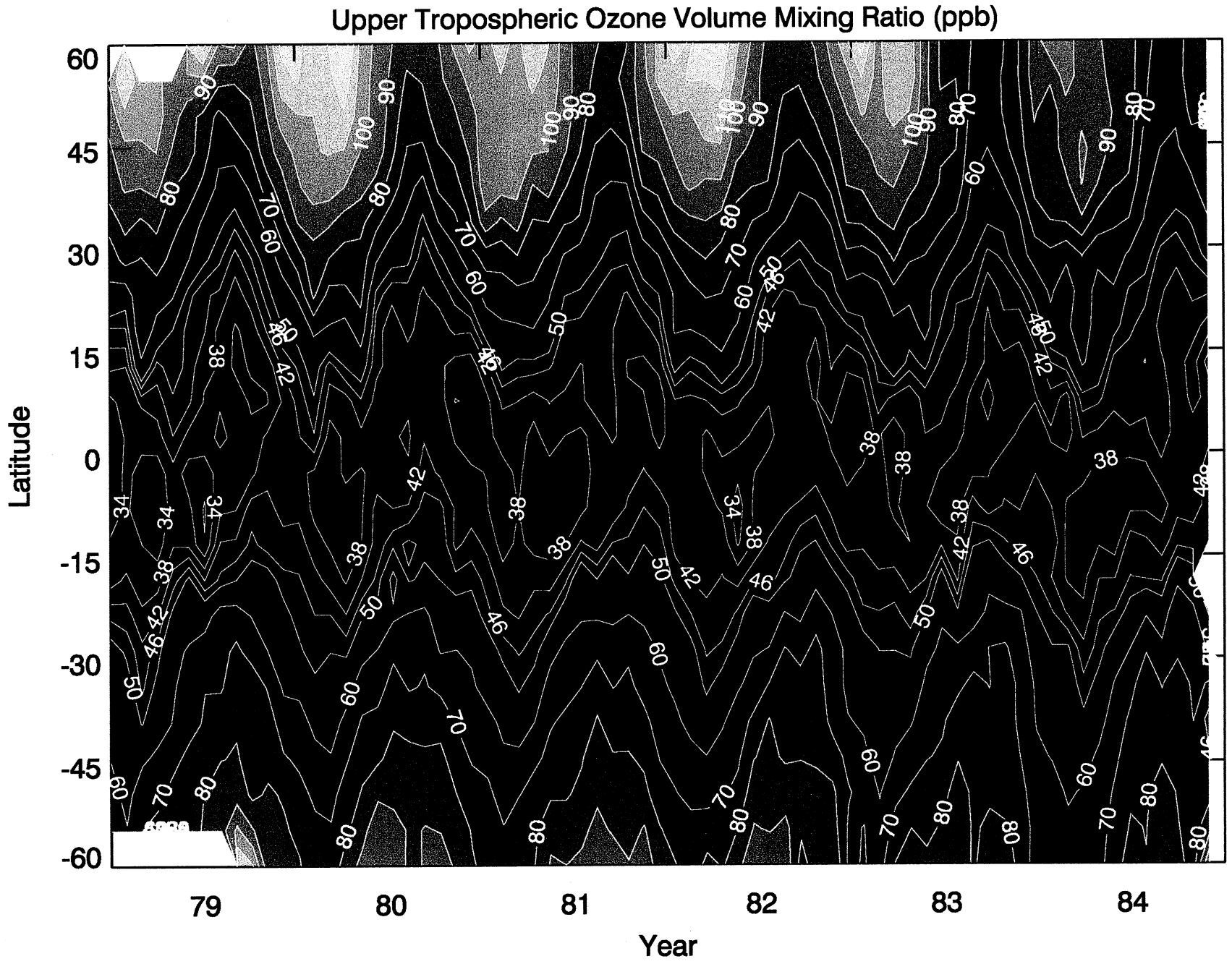
Upper Tropospheric Ozone Volume Mixing Ratio (ppb)
Latitude
60
45
30
15
0
-15
-30
-45
-60
79
80
81
82
83
84
Year

F9

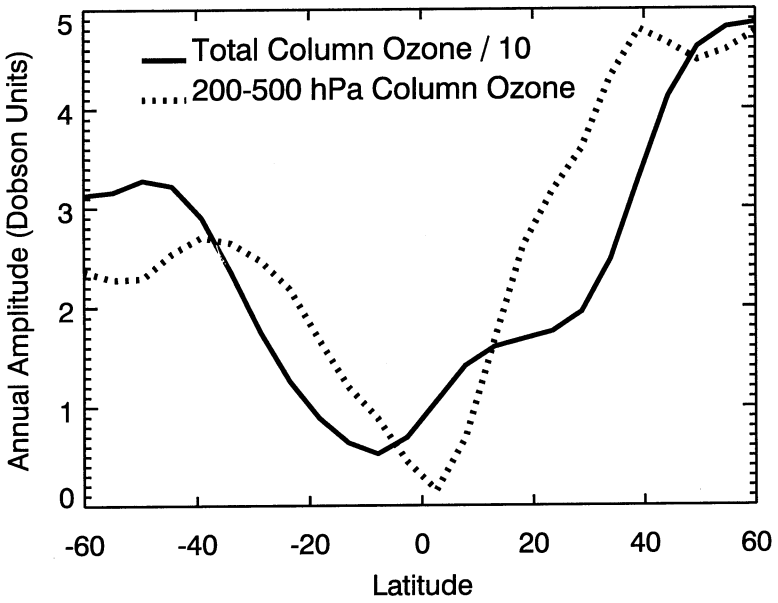
Total Column Ozone / 10
200-500 hPa Column Ozone
Annual Amplitude (Dobson Units)
Latitude
5
4
3
2
1
0
-60
-40
-20
0
20
40
60

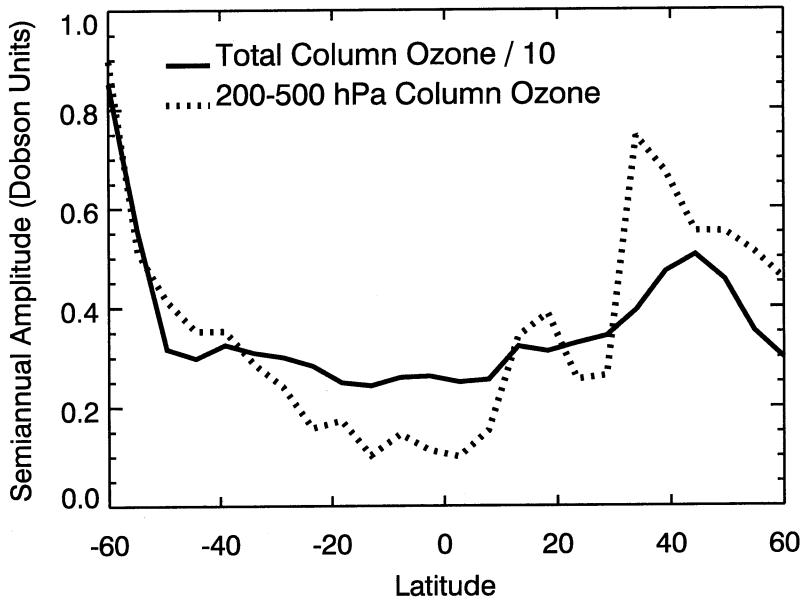
Total Column Ozone / 10
200-500 hPa Column Ozone
Semiannual Amplitude (Dobson Units)
Latitude
1.0
0.8
0.6
0.4
0.2
0.0
-60
-40
-20
0
20
40
60

F10

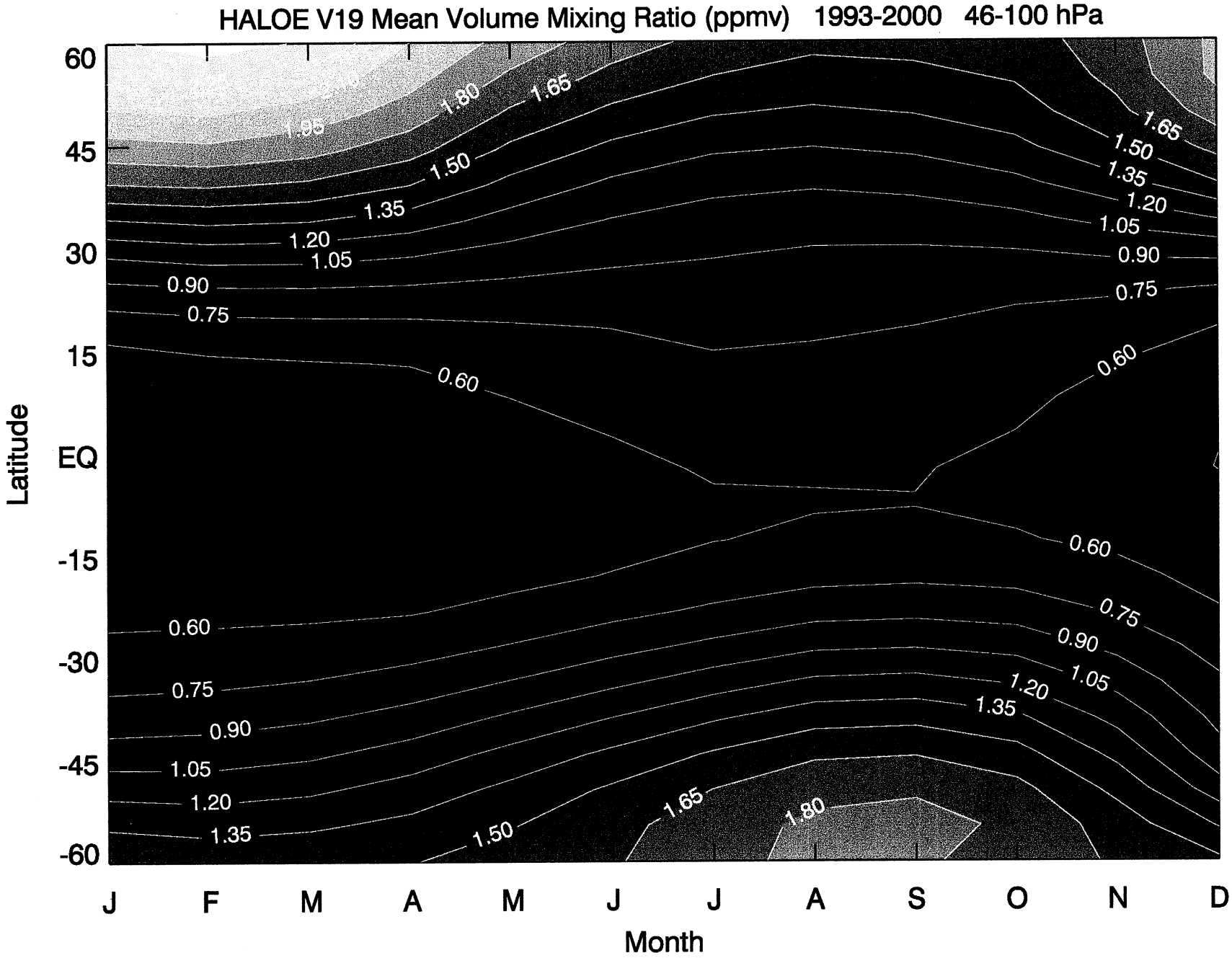
HALOE V19 Mean Volume Mixing Ratio (ppmv) 1993-2000 46-100 hPa
Latitude
60
45
30
15
EQ
-15
-30
-45
-60
J
F
M
A
M
J
J
A
S
O
N
D
Month
1.95
1.80
1.65
1.50
1.35
1.20
1.05
0.90
0.75
0.60

F-11

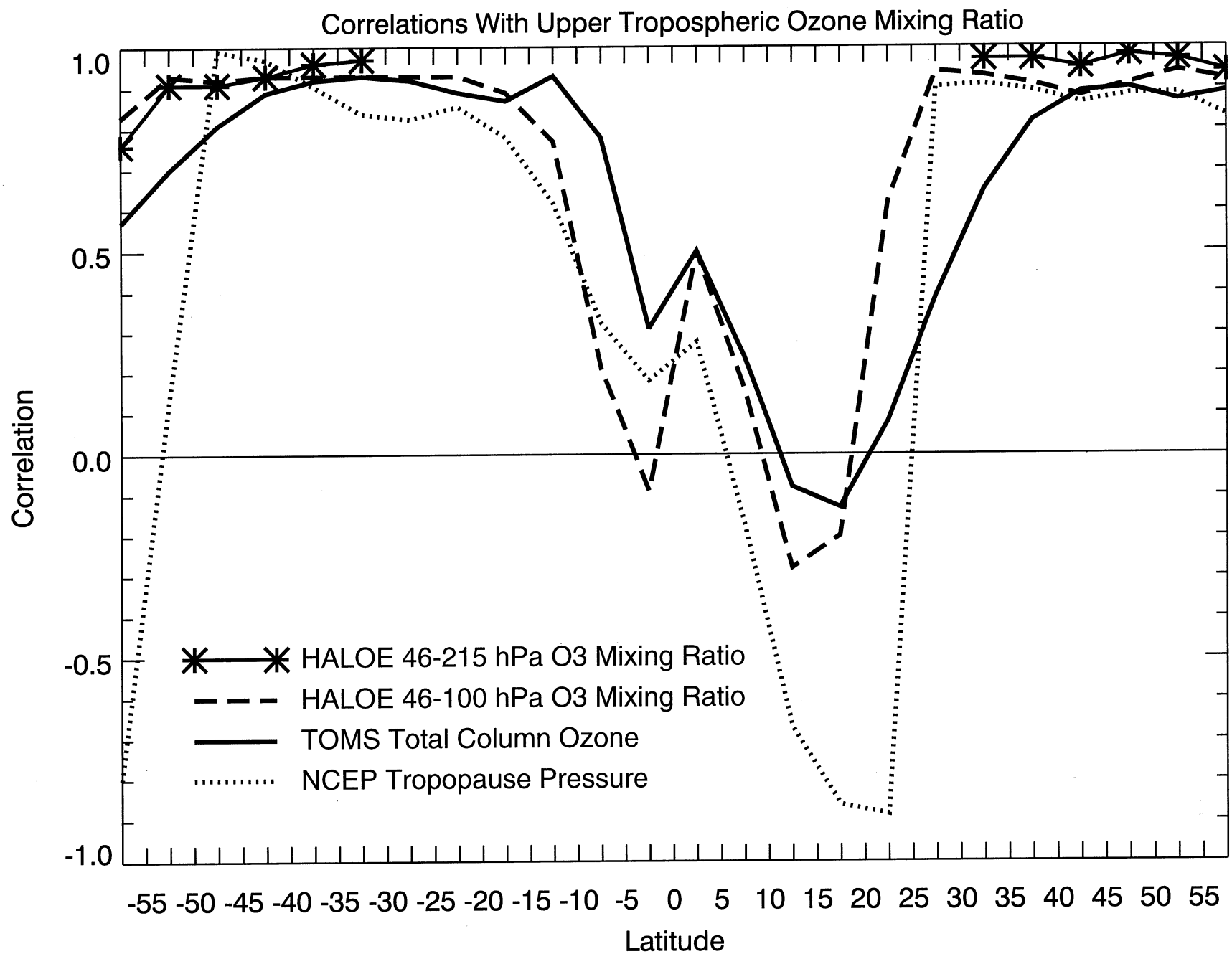
Correlations With Upper Tropospheric Ozone Mixing Ratio
Correlation
1.0
0.5
0.0
-0.5
-1.0
-55 -50 -45 -40 -35 -30 -25 -20 -15 -10 -5 0 5 10 15 20 25 30 35 40 45 50 55
Latitude
HALOE 46-215 hPa O3 Mixing Ratio
HALOE 46-100 hPa O3 Mixing Ratio
TOMS Total Column Ozone
NCEP Tropopause Pressure

F12

Upper tropospheric ozone between latitudes 60S and 60N derived from Nimbus 7 TOMS/THIR Cloud Slicing

Jerald R. Ziemke, Sushil Chandra,
and **P. K. Bhartia**

NASA Goddard Space Flight Center, Code 916, Greenbelt, MD

Popular Summary

This study evaluates the spatial distributions and seasonal cycles in upper tropospheric ozone (pressure range 200-500 hPa) from low to high latitudes (60S to 60N) derived from the satellite retrieval method called "Cloud Slicing". Cloud Slicing is a unique technique for determining ozone profile information in the troposphere by combining co-located measurements of cloud-top pressure and above-cloud column ozone. Measurements of Nimbus 7 Total Ozone Mapping Spectrometer (TOMS) above-cloud column ozone and Nimbus 7 Temperature Humidity Infrared Radiometer (THIR) cloud-top pressure during 1979-1984 were incorporated. In the tropics, derived upper tropospheric ozone shows year-round enhancement in the Atlantic region and evidence of a possible semiannual variability. Upper tropospheric ozone outside the tropics shows greatest abundance in winter and spring seasons in both hemispheres with largest seasonal and largest amounts in the NH. These characteriscs are similar to lower stratospheric ozone. Comparisons of upper tropospheric column ozone with both stratospheric ozone and a proxy of lower stratospheric air mass (i.e., tropopause pressure) from National Centers for Environmental Prediction (NCEP) suggest that stratosphere-troposphere exchange (STE) may be a significant source for the seasonal variability of upper tropospheric ozone almost everywhere between 60S and 60N except in low latitudes around 10S to 25N where other sources (e.g., tropospheric transport, biomass burning, aerosol effects, lightning, etc.) may have a greater role.